that the specular intensity maximum corresponds to the angle φ' equal to 2φ. Besides the specularly reflected intensity diffuse scattering is observed, which might be caused by the surface unevenness and by the back edge of the sample. It is registered most clearly at the angle $\varphi > 14'$, *i.e.* in the case when the specularly reflected intensity may be neglected (see Fig. 4*a*). The experiments showed a weakening of the diffuse intensity when only part of the incident beam reached the crystal back edge (see Fig. 4*b*). This fact showed that the main contribution to the diffuse scattering was due to the scattering at the sample back edge.

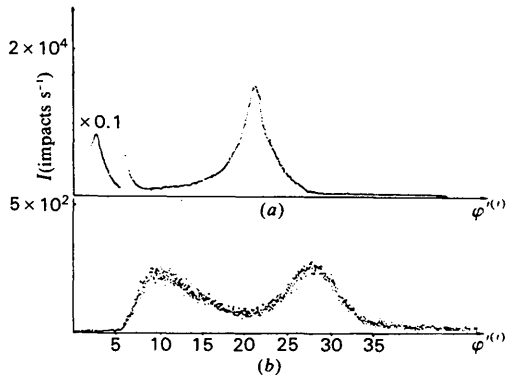

Fig. 4. Distribution of the diffuse intensity for $\varphi = 16'$. (*a*) The crystal covers half of the beam (the forward wave can be seen); (*b*) the crystal covers the whole beam (no forward beam).

Thus, the intensity measurement of the specularly reflected diffracted wave with its exit-angle change has been experimentally realized and the main statements of the theory (Afanas'ev & Melkonyan, 1983) have been confirmed.

The authors express their sincere thanks to Professor A. M. Afanas'ev for his unfailing attention to the work and fruitful discussions, and to D. Novikov for the help in conducting the experiments.

References

AFANAS'EV, A. M. & MELKONYAN, M. K. (1983). *Acta Cryst.* A**39**, 207–210.

GOLOVIN, A. L. & IMAMOV, R. M. (1983). *Phys. Status Solidi A*, **77**, K91–K94.

MARRA, W. C., EISENBERGER, P. & CHO, A. Y. (1979). *J. Appl. Phys.* **50**, 6927–6933.

Acta Cryst. (1984). A**40**, 228–240

Diffuse Scattering in Disordered Ternary Alloys: Neutron Measurements of Local Order in a Stainless Steel $Fe_{0.56}Cr_{0.21}Ni_{0.23}$

BY P. CENEDESE

Institut Laue–Langevin, 156*X*, 38042 *Grenoble CEDEX, France*

AND F. BLEY* AND S. LEFEBVRE

CECM, 15 *rue G. Urbain*, 94400 *Vitry/Seine, France*

(*Received* 24 *May* 1983; *accepted* 1 *November* 1983)

Abstract

The local atomic arrangement in the stainless-steel alloy $Fe_{0.56}Cr_{0.21}Ni_{0.23}$ has been investigated by thermal neutron diffuse scattering from single crystals. The variation of contrast has been obtained by isotopic substitution: three single crystals of different isotopic compositions have been used. The Warren–Cowley parameters of the three heterogeneous pairs have been determined. It is shown that ordering occurs between Ni and Cr atoms. The correlation lengths are small and are of about one cell length. The static displacements are shown to be small. Analysis procedures of diffuse scattering from ternary alloys are developed from neutron scattering and in the Appendix for X-ray scattering.

I. Introduction

During the last ten years, considerable developments have been made in analysing diffusely scattered intensity from mono-crystalline binary alloys since this provides the volume averaged pair atomic correlations by Fourier transformation. These can then be used to model important physical properties such as thermodynamic (pair interaction potentials) and mechanical properties and electrical resistivity.

On the other hand, no direct determination of short-range ordering has been made on multicomponent solid solutions. As a consequence, evolutions of solid

* Present address: INPG–LTPCM (LA29)–ENSEEG, Domaine Universitaire, BP 75, 38042 St Martin d'Hères, France.

0108-7673/84/030228-13$01.50

solutions of practical interest are described merely by assumptions. The aim of this paper is to provide the first experimental evidence of short-range order in stainless-steel-type alloys.

For such an experiment three independent diffuse scattered intensities are needed to measure the Fe–Ni, Fe–Cr and Ni–Cr pair correlations. These are obtained by three experiments on three crystals with identical chemical but different isotopic composition. Even for binary solid solutions, only a few results have been reported by neutron diffuse scattering on single crystals, despite the obvious advantage of the constant scattering length is reciprocal space: for example, on Ni_3Fe (Lefebvre, Bley, Fayard & Roth, 1981), Au_4Mn (Nakashima, Mizuno, Ido, Sato, Mitani & Adachi, 1977) and CuMn (Wells & Smith, 1971; Hirabayashi, Koiwa, Yamaguchi & Kamata, 1978).

The constant scattering length allows us to separate the effects due to order from displacement terms. To determine pair correlations for this ternary alloy, it would also be possible to use only one single crystal and X-ray diffuse scattering, with wavelengths close to the absorption edges of Fe, Cr and Ni. Conditions for this type of experiment, now feasible due to the availability of synchrotron radiation, are described in the Appendix.

Austenitic iron–chromium–nickel alloys are used in nuclear reactors, in cryogenic containers and in high-field superconducting solenoids, because of their low susceptibility to corrosion and for their magnetic properties. These alloys retain a disordered f.c.c. structure from the melt to liquid-helium temperature over a large range of concentration. However, many experiments suggest that some kind of local order exists: Bell, Roser & Thomas (1964) have described contrast experiments using electron microscopy on superdislocations in Fe–20 wt% Cr–30 wt% Ni and 40 wt% Ni which confirm earlier suggestions of the existence of some ordering (Douglass, Thomas & Roser, 1964). Pairs of dislocations have also been observed more recently in $Fe_{0.57}Cr_{0.20}Ni_{0.23}$ and $Fe_{0.54}Cr_{0.20}Ni_{0.26}$ (Lefèvre, 1980).

$Fe_{0.6}Cr_{0.2}Ni_{0.2}$ is a transition composition for magnetic properties. Warners & King (1976) have shown that this alloy changes from anitferromagnetic to ferromagnetic at low temperature on varying the composition close to this point. In fact, in this transition zone, the alloy exhibits superparamagnetism, which the authors explain by small ferromagnetic clusters in an antiferromagnetic matrix.

Heterogeneities of the microstructure and particularly short-range order have been invoked by Dimitrov, Tenti & Dimitrov (1981) in order to explain a peak of resistivity with annealing temperature in Fe–16 wt% Cr–20 wt% Ni and 25 wt% Ni, near 823 K in unirradiated samples, and near 603 K in samples having undergone low-temperature irradiation with fast neutrons.

A weak increase of the residual resistivity has been found in $Fe_{0.57}Cr_{0.20}Ni_{0.23}$ and $Fe_{0.54}Cr_{0.20}Ni_{0.26}$ (Protopopoff, 1981) after 5 h annealing at 773 K. In the same alloys, an increase of thermoelectric power has been found by Pelletier (1981) after 10 h annealing at 773 K.

In the same range of concentration, Bendick & Pepperhoff (1981) have found specific heat anomalies near 503 and 873 K. But in this case, owing to kinetic considerations, these authors did not attribute any of these anomalies to short-range order.

Considering all these results, a quantitative measurement of local order in FeCrNi alloys is necessary to determine what type of local atomic arrangement actually exists.

II. General equations

The general equations for scattering from a multicomponent and multisublattice solid solution have been given by Hayakawa & Cohen (1975). Following their treatment, the total diffuse intensity per atom from an N-component cubic alloy can be expanded up to the second-order displacements as

$$\begin{aligned} I(h_1, h_2, h_3) = & \sum_{a=1}^{N-1} \sum_{b>a}^{N} x_a x_b |f_a - f_b|^2 \tilde{\alpha}^{ab}(h_1, h_2, h_3) \\ & + \sum_{a=1}^{N} \sum_{b\geq a}^{N} x_a x_b (f_a f_b^* + f_a^* f_b) \\ & \times [h_I Q_I^{ab}(h_1, h_2, h_3) \\ & + (h_I)^2 R_I^{ab}(h_1, h_2, h_3) \\ & + h_I h_J S_{I,J}^{ab}(h_1, h_2, h_3)] (J > I), \end{aligned} \tag{1}$$

where h_1, h_2, h_3 are the coordinates of the reciprocal-lattice vector $\mathbf{h}$, x_a, x_b = the concentration of atoms (a, b, indices describing the chemical species), f_a = the atomic scattering factor of atom a, reduced by its Debye–Waller factor, I, J are Cartesian indices and implicitly refer to a summation.

Expression (1) differs from Hayakawa's in that there is only one atom per cell and the Laue monotonic is not factorized in order to maintain the dependence of each term with complex atomic scattering factor.

The different functions are

$$\begin{aligned} \tilde{\alpha}^{ab}(h_1, h_2, h_3) = & \sum_{l=-\infty}^{l=+\infty} \sum_{m=-\infty}^{m=+\infty} \sum_{n=-\infty}^{n=+\infty} \alpha^{ab}(l,m,n) \\ & \times \cos(2\pi h_1 l) \cos(2\pi h_2 m) \\ & \times \cos(2\pi h_3 n) \end{aligned} \tag{2}$$

$$\begin{aligned} Q_x^{ab}(h_1, h_2, h_3) = & -2\pi \sum_{l=-\infty}^{l=+\infty} \sum_{m=-\infty}^{m=+\infty} \sum_{n=-\infty}^{n=+\infty} F^{ab}(l,m,n) \\ & \times \langle x_{l,m,n}^{ab} \rangle \sin(2\pi h_1 l) \\ & \times \cos(2\pi h_2 m) \cos(2\pi h_3 n) \end{aligned} \tag{3}$$

$$R_x^{ab}(h_1, h_2, h_3) = 4\pi^2 \sum_{l=-\infty}^{l=+\infty} \sum_{m=-\infty}^{m=+\infty} \sum_{n=-\infty}^{n=+\infty} F^{ab}(l,m,n) \times \langle (x_{l,m,n}^{ab})^2 \rangle \cos(2\pi h_1 l) \times \cos(2\pi h_2 m) \cos(2\pi h_3 n) \quad (4)$$

$$S_{xy}^{ab}(h_1, h_2, h_3) = 8\pi^2 \sum_{l=-\infty}^{l=+\infty} \sum_{m=-\infty}^{m=+\infty} \sum_{n=-\infty}^{n=+\infty} F^{ab}(l,m,n) \times \langle x_{l,m,n}^{ab} Y_{l,m,n}^{ab} \rangle \sin(2\pi h_1 l) \times \sin(2\pi h_2 m) \cos(2\pi h_3 n) \quad (5)$$

$$\left.\begin{aligned} F^{aa}(l,m,n) &= \frac{1}{2x_a}\left[x_a + \sum_{b \neq a} x_b \alpha^{ab}(l,m,n)\right] \\ F^{ab}(l,m,n) &= 1 - \alpha^{ab}(l,m,n) \qquad a \neq b. \end{aligned}\right\} \quad (6)$$

Thus, two kinds of terms become apparent: firstly, the periodic modulations which depend only on the structure of the sample and, secondly, the coefficients of these functions which depend on the 'atomic scattering factors'. These coefficients must have different values if the periodic pair functions are to be separable and hence must be varied in different experiments.

In (2) to (5), $\alpha^{ab}(l,m,n)$ is one of the $[N(N-1)/2]$ Warren–Cowley local order parameters introduced by de Fontaine (1971) for an N-multicomponent alloy. Terms between brackets have the same meaning as for the binary case. They are just the conventional displacement terms from the average lattice value with atom A at the site l,m,n and B at the origin.

We note that (1) retains the binary expression form and consequently the detailed symmetry relations described by Gragg (1970) and Gragg & Cohen (1971) hold with the same assumptions.

Differences between binary intensity expression and (1) arise because pair parameters appear in linear combinations and several independent measurements are needed to separate them. The details of the separation procedure will be discussed below.

To obtain different 'atomic scattering factors' for the same chemical species, we can use two different methods.

(1) In neutron diffuse scattering, the nuclear scattering lengths of elements depend on the isotope used and in some fortunate cases there exist enough isotopes of different elements for independent measurements to be made.

(2) In X-ray scattering, the atomic scattering factor has significant variations in the vicinity of an absorption edge of the element as a function of the incident X-ray wavelength.

As has been suggested by Ramesh & Ramaseshan (1971), the anomalous dispersion corrections may be used to separate different terms in the diffuse scattering. Owing to the availability of synchrotron radiation, these kinds of experiments may now be carried out.

Finally, since, for neutron scattering, the scattering lengths do not vary with angle whilst, for X-rays, the atomic scattering factors do, it is necessary to separate each case and treat it accordingly. The neutrons are treated in the text and the case for X-rays is discussed in the Appendix.

III. Thermal neutron scattering

Two terms have to be considered: nuclear and magnetic scattering. The nuclear term is scattering-angle independent since the nuclei have negligible spatial extension compared to the neutron wavelength. The magnetic term depends on scattering angle because it is due to the interaction of the neutron spin and the outer electrons. This term is only significant for magnetically ordered alloys; it may be suppressed in soft ferromagnetic materials by applying a suitable magnetic field. In the following, this term will not be considered. The only remaining scattering-angle-dependent term occurs because the atoms vibrate about their mean lattice positions (Debye–Waller factor).

Assuming a mean 'Debye–Waller' factor for each type of atom, we write

$$b_a(\mathbf{h}) = b_a \exp[-M_a(\mathbf{h})] \simeq b_a \exp[-M(\mathbf{h})]$$

and we divide the diffuse scattered intensity on each reciprocal point by $\exp -2M(\mathbf{h})$. We obtain the following expression for the coherent differential cross section

$$\frac{d\sigma}{d\Omega} \exp[2M(\mathbf{h})] = I_{SRO}(\mathbf{h}) + h_I Q_I(\mathbf{h}) + (h_I)^2 R_I(\mathbf{h}) + h_I h_J S_{I,J}(\mathbf{h}), \quad (7)$$

where

$$I_{SRO}(\mathbf{h}) = \sum_{a=1}^{N-1} \sum_{b>a}^{N} x_a x_b (b_a - b_b)^2 \tilde{\alpha}^{ab}(\mathbf{h}) \quad (8a)$$

and

$$Q_x(\mathbf{h}) = \sum_{a=1}^{N} \sum_{b \geq a}^{N} x_a x_b b_a b_b Q_x^{ab}(\mathbf{h}). \quad (8b)$$

The terms I_{SRO}, Q_x being periodic in reciprocal space as in binary alloys, it is possible to apply the treatment of Borie & Sparks (1971; hereafter BS) [Gragg, 1970; Gragg & Cohen, 1971] without further assumptions.

Let us now look at the short-range-order intensity. The separation of each pair intensity $\tilde{\alpha}_{ab}(\mathbf{h})$ (or by Fourier transform of each short-range-order pair parameter) can be achieved if $N(N-1)/2$ independent diffuse scattering measurements are provided by the different samples.

For a ternary alloy, let us call $I_{SRO,i}(\mathbf{h})$ the short-range-order modulation found by the BS separation method for the ith experiment, and $b_{A,i}$ the coherent

scattering length of the A-atom isotope in the ith sample. The pair intensities are solutions of a 3×3 linear system of equations

$$I_{\mathrm{SRO},i}(\mathbf{h}) = x_A x_B (b_{A,i} - b_{B,i})^2 \tilde{\alpha}^{AB}(\mathbf{h}) + x_A x_C (b_{A,i} - b_{C,i})^2 \tilde{\alpha}^{AC}(\mathbf{h}) + x_B x_C (b_{B,i} - b_{C,i})^2 \tilde{\alpha}^{BC}(\mathbf{h}). \quad (9)$$

These expressions can be summarized under the matrix fom

$$\boldsymbol{\sigma}(\mathbf{h}) = A\tilde{\boldsymbol{\alpha}}(\mathbf{h}),$$

where $\boldsymbol{\sigma}$ represents the vector of components $I_{\mathrm{SRO},i}$ and the A matrix consists of elements $a_{i,j}$, where the subscripts i refer to the different experiments or samples and the subscripts j refer to the different pairs.

The reliability of the solutions of the previous linear system is highly dependent upon the choice of isotopes. If the system is ill conditioned, small statistical errors $\Delta\sigma$ in the short-range-order intensities I, or small variations of the A-matrix elements ($b_A \rightarrow b_A + \Delta b_A$) would have a large effect on the solutions $\tilde{\alpha}$ of the equations.

Ill conditioning with respect to linear systems occurs when the matrix is nearly singular. The determinant of the normalized equations obtained by dividing the ith row by $(\sum_{j=1}^{n} a_{ij}^2)^{1/2}$ can be used as a test for ill conditioning (Westlake, 1968). If the absolute value of this determinant is small compared to 1, the system is ill conditioned.

Another suitable criterion is given by the Turing number $N(A)$, defined for a matrix of order n by

$$N(A) = n^{-1}\|A\| \times \|A^{-1}\|, \quad (10)$$

where

$$\|A\| = \left[\sum_{i=1}^{i=3}\sum_{j=3}^{j=3} (a_{i,j})^2\right]^{1/2}. \quad (10a)$$

The Turing number of a matrix, the coefficients of which are chosen at random from a normal population, is of order $\sqrt{n}$. A change $\Delta\sigma$ due to the uncertainty in short-range-order intensity causes a change in $\tilde{\alpha}$ values such that

$$\|\Delta\tilde{\boldsymbol{\alpha}}\|/\|\tilde{\boldsymbol{\alpha}}\| \leq nN(A)[\|\Delta\boldsymbol{\sigma}\|/\|\boldsymbol{\sigma}\|]. \quad (10b)$$

Hence, $N(A)$ is a measure of conditioning (Westlake, 1968).

In the present experiment on the stainless-steel alloy $Fe_{0.56}Cr_{0.21}Ni_{0.23}$, three samples of various isotopic compositions are used. The determinant of the normalized matrix calculated from the neutron characteristics given in Tables 1 and 2 is equal to 0·3, which is reasonably good. For example, determinations of partial structure factors in amorphous materials are commonly made with such a determinant less than 0·1. The Turing number is equal to 7; it can be compared to $\sqrt{n} = 1{\cdot}732$. This means that the system is reasonably well conditioned.

Table 1. *Isotopic composition and scattering lengths of the isotopes used*

The scattering lengths are computed from the data of Koester & Rauch (1981), for the particular isotopic compositions.

Isotope	Isotopic composition (at. %)					Scattering length (fm)
Natural iron						9·54 (6)
Iron 54	^{54}Fe	^{56}Fe	^{57}Fe			
	99·65	0·33	0·02			4·2 (1)
Chromium 52	^{50}Cr	^{52}Cr	^{53}Cr	^{54}Cr		
	0·1	99·5	0·3	0·1		4·88 (2)
Nickel 62	^{58}Ni	^{60}Ni	^{61}Ni	^{62}Ni	^{64}Ni	
	1·17	0·80	0·19	97·7	0·14	−8·3 (2)
Nickel 58	^{58}Ni	^{60}Ni	^{61}Ni	^{62}Ni	^{64}Ni	
	99·8	0·15	<0·01	0·04	0·01	14·37 (10)

According to the inequality (10*b*), the uncertainty on $\tilde{\alpha}$ decreases with decreasing uncertainty on the measurements $\Delta\sigma$. This means that the Laue monotonic scattering of each sample must have a significant value.

To extract explicitly each pair-displacement term additional measurements are needed. The expression for the intensity (1) involves 57 independent pair parameters [in general $N(5N+4)$] including the Cartesian decomposition of modulations such as Q. This number is reduced to $[N(5N+4)-3]=54$ by inclusion of the three Cartesian relations of the volume conservation of each shell. The BS treatment allows only ten sets of independent parameters to be determined from each sample and hence to determine 54 individual independent parameters, measurement would be required on $N(N+1)/2=6$ different samples.

It will be noted that, in the binary case, three samples are needed in order to determine all displacement terms up to second order.

IV. Experiment

(*A*) *Samples*

The three cylindrical-shaped single crystals (5·5 mm diameter and 6 mm height) were grown simultaneously in alumina crucibles under a purified argon atmosphere using a Bridgman technique. The constituents used are as follows:

first sample: natural Fe, isotope 62 of Ni, isotope 52 of Cr;
second sample: isotope 54 of Fe, isotope 62 of Ni, isotope 52 of Cr;
third sample: natural Fe, isotope 58 of Ni, isotope 52 of Cr.

These samples are respectively labelled: Inox 1, Inox 2 and Inox 3. The isotopic composition and the scattering length of each isotope are given in Table 1.

Table 2. *Atomic composition and differential cross sections for pair Laue monotonic, total Laue monotonic and total incoherent, of each sample*

	Atomic composition (at. %)			Laue monotonic (fm^2 $atom^{-1}$ sr^{-1})			Total incoherent differential cross section (fm^2 $atom^{-1}$ sr^{-1})
	Fe	Ni	Cr	Fe–Ni	Fe–Cr	Ni–Cr	Total
Inox 1	56·06	23·02	20·92	41·07 (120)	2·55 (9)	8·37 (28)	51·99 (157)	3·89
Inox 2	56·14	23·07	20·79	20·24 (98)	0·05 (2)	8·33 (28)	28·62 (128)	1·95
Inox 3	56·11	23·04	20·85	3·02 (20)	2·54 (9)	4·33 (11)	9·89 (40)	2·67

The precise sample atomic compositions, given in Table 2, have been evaluated from pure metal weighing before a rapid plasma fusion, and with the assumption that the weight loss of each sample is due to chromium evaporation (approximately 0·2% of the total weight).

Finally, the samples were spark machined and electropolished before annealing for 1 h at 1273 K and 10 h at 773 K under 1·3 μPa vacuum. The homogeneity of the samples, which was checked by X-ray analysis in a scanning electron microscope, is within 1%

The resulting Laue monotonic pair values $x_a x_b (b_a - b_b)^2$ and the incoherent differential cross section of each sample are listed in Table 2. The incoherent cross sections, which mainly arise from the nuclear incoherency, do not include the paramagnetic contribution which is very low. The incoherent scattering accounts for, respectively, 7·5, 6·8 and 27% of the total Laue monotonic. It should be noted that isotope 52 of chromium has been used instead of the natural element since the nuclear incoherent cross section of the latter is increased by the incoherent nuclear spin scattering of isotope 53.

For the chosen composition, the alloy is f.c.c. at any temperature between the melting point (Schurmann & Brauckmann, 1977), to the lowest temperature (Warnes & King, 1976). The cell parameter is 3·583 Å, according to Pearson (1958).

(*B*) *Intensity measurements*

The experiments were performed at room temperature on the three-axis four-circle diffractometer D10 at the ILL (Grenoble). The diffuse scattered intensities were measured with an ^{3}He counter located behind a graphite analyser which eliminates the inelastic scattering owing to its resolution $\Delta\lambda/\lambda = 0{\cdot}1$ for the neutron wavelength used (1·29 Å).

The low mosaicity of the crystals and the good resolution of the diffractometer allowed measurements close to the Bragg peaks, at a distance $\Delta h = 0{\cdot}1$ in reciprocal parameter units.

The intensities were corrected for background intensity (denoted I_{BG}) and absorption. The linear absorption coefficient of each sample was experimentally measured. For each position in reciprocal space, a transmission factor T_i is calculated, according to the precise shape of each sample. The intensities are then converted to scattering-cross-section units from measurements of the purely incoherent scattering intensity I_V of a hollow cylinder of polycrystalline vanadium, whose transmission factor is T_V.

With the above notation, the coherent differential cross section $(d\sigma/d\Omega)_i$ of sample i is related to the measured intensities I_i and I_V by

$$\left(\frac{d\sigma}{d\Omega}\right)_i = \frac{N_V}{N_i}\frac{\sigma_V}{4\pi}\frac{T_V}{T_i}\frac{\exp -2M_V}{\exp -2M_i} \times \frac{(I_i - T_i I_{BG})}{(I_V - T_V I_{BG})}\frac{\sigma_i^{inc}}{4\pi}, \quad (11)$$

where $\sigma_V/4\pi = 5{\cdot}06/4\pi$ is the differential incoherent cross section of vanadium, $M_V = B_V(\sin^2\theta)/\lambda^2$ is the Debye–Waller factor of vanadium, $B_V = 0{\cdot}57$ Å^2, $M_i = B_i(\sin^2\theta)/\lambda^2$ is the mean Debye–Waller factor of the alloy; the value $B_i = 0{\cdot}35$ Å^2 is used in a first step; N_V, N_i are the numbers of atoms of vanadium and of samples i.

For Inox 1, the intensity is measured over the whole volume needed to separate short-range order from first- and second-order displacement modulations. This volume extends from 100 to 203 and 222 in reciprocal space, as described by Gragg (1970) and Gragg & Cohen (1971); it includes 1486 measurement points. For 5 min counting time the number of detected counts ranges from 160 (near a maximum, for example the 110 position) to 110 near a minimum. In comparison, the background count is 8.

Since the total intensity map shows only very small displacement effects, the volume of measurement was reduced for the other two samples (Inox 2 and Inox 3). This volume, which enables the first-order displacement term to be measured extends from 001 to 202 as previously described by Metcalfe & Leake (1975). The number of points was reduced to 576, and the counting time increased to 10 min. The number of detected counts ranges from 220 to 120 for Inox 2 and is still lower for Inox 3 for which the number of counts ranges from 140 to 90. The background is now 27 counts.

The effect of statistical errors on the coherent differential cross section is evaluated, taking into account background intensity and incoherent scattering, assuming a statistical error of $\sqrt{N}$ counts; the resulting errors range from 8 to 11% for Inox 1, 8 to 12% for Inox 2, 11 to 30% for Inox 3.

The experimental iso-intensity curves are given in Fig. 1 for the three alloys. They are obtained by interpolation between the measured points. Statistical errors cannot be taken into account in these contours. The modulations of the Laue diffuse scattering, whose values are given in Table 2, are very weak in all three samples. Maxima appear near the 100 and 110 positions which are the positions of cubic primitive 'superstructure' reflections.

The modulation of the diffuse intensity along superstructure fundamental lines (Fig. 2) is similar for Inox 1 and Inox 2. Since the Laue diffuse scattering of Inox 1 is dominated by the Fe–Ni term, this indicates very little order between nickel and iron. Despite large statistical errors, the observed modulations are seen to be meaningful.

V. Separation of local order intensity: adaptation of the method of Borie & Sparks (1971) for low counting rates

In the 'classical' Gragg (1970) analysis, which is a practical adaptation of the BS method, the short-range-order intensity at one point $h_1h_2h_3$ is obtained from a combination of diffuse intensities measured at five points, in order to extract displacement terms up to second order:

[1]: h_1, h_2, h_3; [2]: $2-h_1, h_2, h_3$; [3]: $2+h_1, h_2, h_3$;

[4]: $h_1, h_2, 2-h_3$; [5]: $2-h_1, h_2, 2-h_3$.

These sets of points are sub-volumes of the whole volume in reciprocal space. Let $I(1)$, $I(2), \ldots, I(5)$ be the corresponding diffuse intensity values. The second-order displacement modulation components R_x and S_{xy}, at point $h_1h_2h_3$, are first obtained directly by the two equations

$$R_x(1) = I(2) + I(3) - 2I(1) \tag{12}$$

$$S_{xy}(1) = [I(1) - I(2)] + [I(5) - I(4)]. \tag{13}$$

Then $Q_x(1)$ at point $h_1h_2h_3$ may be determined:

$$Q_x(1) = \tfrac{1}{2}[I(1) - I(2)] - h_2 S_{xy}(1) - h_3 S_{zx}(1) - 2(1-h_1)R_x(1). \tag{14}$$

The short-range-order intensity, at point $h_1h_2h_3$ is the last result:

$$I_{SRO}(1) = I(1) - \sum h_i Q_i(1) - \sum h_i h_j S_{ij}(1) - \sum_i h_i^2 R_i(1). \tag{15}$$

In this 'classical' method, some steps in the calculation have to be improved when the statistical error is large.

(1) After the separation, I_{SRO} is obtained in volume [1] which contains 480 points in this case; this volume is larger than the minimum volume for SRO determination in f.c.c. structures which contains 160 points.

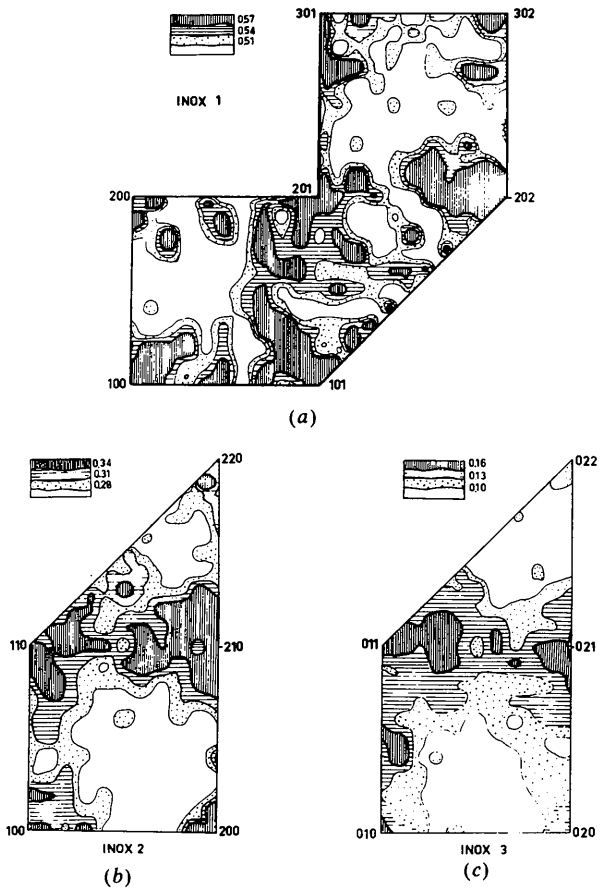

Fig. 1. Maps of experimental diffuse intensity, corrected with equation (1), in a (001) plane for the three samples. (Differential cross sections in 100 fm^2 atom^{-1} sr^{-1}.)

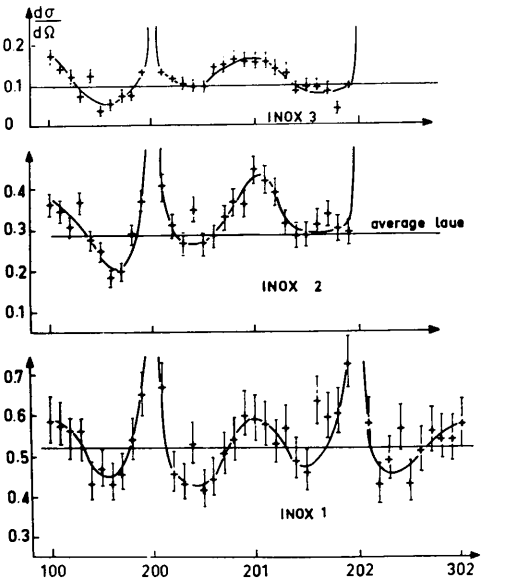

Fig. 2. Experimental intensity, in 100 fm^2 atom^{-1} sr^{-1}, along superstructure fundamental lines, for the three samples.

Thus we can average equivalent points before Fourier transforming.

(2) The volumes [3], [4] and [5] are used only to extract second-order displacment terms, but, once this is done, the remaining intensities can be used to extract Q_x and I_{SRO}. So, more points can be used, and averaged when equivalent, to decrease statistical errors; this is particularly useful when displacements are neglected.

Thus, after the classical separation of second-order displacement terms, Q_x is computed in four different ways, according to the relations: $I(1)$–$I(2)$; $I(3)$–$I(1)$; $I(4)$–$I(5)$; $I(2)$–$I(5)$. The average values of Q_x are calculated for each point $(h_1h_2h_3)$ of the minimum repeat volume for Q_x, and then the contribution of first-order displacement terms is obtained in the whole measurement volume in order to give I_{SRO}. The short-range order I_{SRO} is then known at 1486 points and is calculated by averaging all the equivalent points. the number of equivalent points depends on their symmetry; it varies from 3 to 20, the average value being 10; so, for most of the points, the statistical error is reduced by a factor of 3.

This procedure is applied for Inox 1; for the other two samples, it is assumed that S_{xy} and R_x vanish. The number of experimental points is reduced to 576, and consequently the number of equivalent points of I_{SRO} is reduced to about 3, and the statistical error is reduced by a factor of 1·7.

The displacement intensities are the result of linear combinations of measured intensities. When these values are very weak, the various differences depend mainly on the statistical error. To test whether these intensities have a physical meaning, we have compared, for each measured point, the experimental intensity and the calculated one synthesized from I_{SRO}, Q_x, R_x and S_{xy}. We have computed the agreement ratio R for the following three cases:

(*a*) the first- and second-order displacements are taken into account;

(*b*) the second-order displacement terms are neglected;

(*c*) the first- and second-order displacements are neglected.

Table 3. *Values of the agreement ratio R for the different methods of separation of* I_{SRO}, I_{D_1}, I_{D_2} *described in the text*

Sample	Hypothesis	Classical	Modified
Inox 1	*a*	0·3871	0·4883
	b	0·2746	0·1566
	c	0·1616	0·1221
Inox 2	*b*	0·2383	0·2138
	c	0·1817	0·1520
Inox 3	*b*	0·4280	0·4021
	c	0·3545	0·3113

The agreement ratio is defined as

$$R = \left[\frac{\sum_{\{h_1h_2h_3\}} [I_{exp}(h_1h_2h_3) - I_{cal}(h_1h_2h_3)]^2}{\sum_{\{h_1h_2h_3\}} [I_{exp}(h_1h_2h_3)]^2} \right]^{1/2} . \quad (16)$$

The agreement ratios, calculated with both methods – classical and modified BS method – are compared in Table 3.

For weak displacement effects, and a low counting rate, it is better to neglect second-order displacements for both methods. If they are not neglected, the modified method is worse than the classical one. Indeed, distant points in reciprocal space are used to determine average I_{SRO} and Q_x, and then the errors on R_x and S_{xy} modulations are amplified by the multiplying factors such as h_i^2 or h_ih_j.

If the second-order terms are neglected, the agreement ratio is improved in the modified method, owing to the large number of ways to determine the modulations Q_x and I_{SRO}. This conclusion is not so clear for Inox 2 and Inox 3 where the total number of measurement points is reduced. Finally, the values of the agreement ratio, especially for the modified method, in case *c* are in good agreement with the evaluation of the statistical error for each sample.

Short-range-order intensity maps, for the three samples, are shown in Fig. 3. Broad maxima occur near 'superstructure' positions of the primitive cubic structure, and also near Bragg peaks. In the sample Inox 3, the superstructure maxima extend along superstructure–superstructure lines. The averaging of

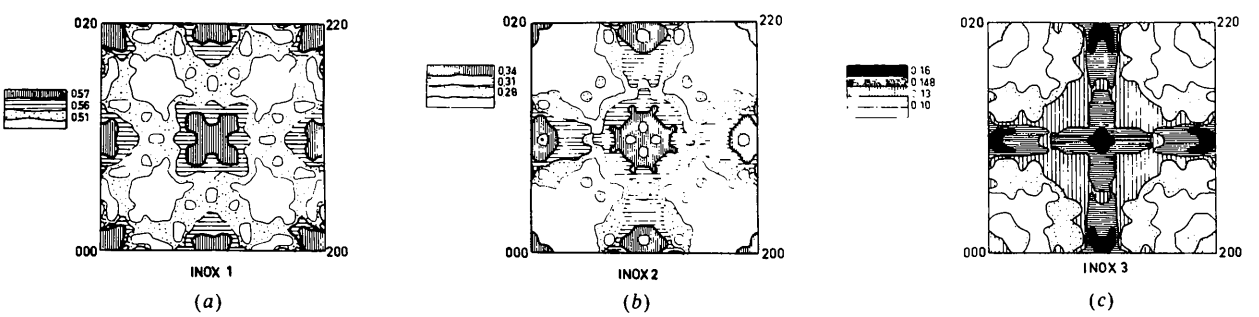

Fig. 3. Short-range-order intensity maps in a (001) plane for the three samples. Modified Sparks & Borie method and hypothesis *b* have been used.

Table 4. *Fourier coefficients a^i_{lmn} of the short-range intensity for each sample*

Units are 100 fm^2 atom^{-1} Sr^{-1}.

Hypothesis b = second order displacement terms equal to 0

lmn	Inox 1	Inox 2	Inox 3
000	0·4983	0·2641	0·0985
110	−0·0009	−0·0070	−0·0050
200	0·0129	0·0100	0·0078
211	0·0012	0·0005	0·0016
220	0·0012	0·0006	0·0003
310	0·0003	−0·0004	0·0002
222	0·0017	0·0012	−0·0005
321	0·0011	0·0004	−0·0002
400	0·0016	0·0008	0·0017

Hypothesis c = all displacement terms equal to 0

lmn	Inox 1	Inox 2	Inox 3
000	0·4911 (15)	0·2688 (16)	0·0965 (9)
110	−0·0024 (4)	−0·0057 (4)	−0·0046 (3)
200	0·0123 (6)	0·0116 (6)	0·0075 (4)
211	0·0010 (3)	0·0006 (3)	0·0012 (2)
220	0·0003 (4)	0·0007 (4)	−0·0001 (2)
310	0·0003 (3)	0·0003 (3)	−0·0007 (2)
222	0·0013 (5)	0·0015 (5)	−0·0002 (3)
321	0·0005 (2)	0·0000 (2)	0·0000 (1)
400	0·0012 (6)	0·0018 (6)	0·0009 (4)

equivalent points therefore allows us to have better statistics, and the modulations of short-range-order intensity become clearer. The displacement intensities are very weak and will be neglected.

VI. Local order

In a ternary alloy, the pair parameters α^{ab}_{lmn} are obtained by two equivalent methods:

Separation of short-range-order intensities corresponding to each pair of atoms, by solving a system of linear equations for each point of reciprocal space, preceding the Fourier transform, as explained previously;

Fourier transform of the short-range-order intensity of each sample, a resolution of a set of linear equations. The Fourier coefficients a_{lmn} are related to α_{lmn} by the same contrast matrix as in the first case:

$$\mathbf{a}_{lmn} = A\boldsymbol{\alpha}_{lmn}.$$

The parameters a_{lmn} of each sample are given in Table 4, for the two better treatments previously explained: (*b*) with first-order displacements; (*c*) with no displacement at all.

The values of pair parameters α^{ab}_{lmn} are given in Table 5. Their variation with interatomic distance $(l^2+m^2+n^2)^{1/2}$ is shown in Fig. 4. The scattering lengths *b* of the elements and, thus, the contrast matrix have been chosen within the limits of accuracy, in order to give values of α^{ab}_{000} as close as possible to 1.

According to the results of Table 5, the most striking feature is that pair correlations between Ni and Cr are large in the first two shells. The values of other

Table 5. *Pair short-range order parameters α^{AB}_{lmn}*

Hypothesis b = second order displacement terms equal to 0

lmn	Fe–Ni	Fe–Cr	Ni–Cr
000	0·975	1·075	0·938
110	0·025	0·027	−0·148
200	0·002	0·096	0·119
211	−0·002	0·044	0·012
220	0·002	0·007	0·002
310	0·001	0·018	−0·006
222	0·006	−0·025	0·001
321	0·004	−0·004	−0·004
400	−0·002	0·045	0·013

Hypothesis c = all displacement terms equal to 0

lmn	Fe–Ni	Fe–Cr	Ni–Cr
000	0·959 (7)	0·959 (52)	0·973 (30)
110	0·017 (2)	−0·009 (14)	−0·113 (8)
200	−0·002 (3)	0·043 (20)	0·148 (12)
211	−0·002 (1)	0·029 (10)	0·012 (6)
220	0·001 (2)	−0·017 (13)	0·007 (8)
310	0·003 (1)	−0·024 (10)	−0·003 (6)
222	0·003 (2)	−0·033 (17)	0·012 (10)
321	0·002 (1)	0·005 (6)	−0·004 (4)
400	−0·002 (3)	−0·009 (20)	0·026 (12)

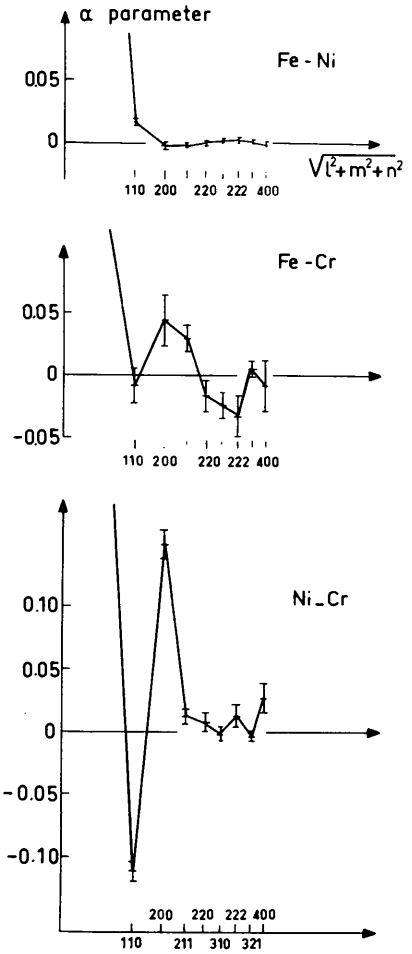

Fig. 4. Pair short-range-order parameters α^{AB}_{lmn} *versus* interatomic distance. Modified Sparks & Borie method and hypothesis *b* have been used.

pair-correlation parameters are weak and will be discussed further, when errors will be evaluated.

The pair short-range-order intensities, calculated using the first eight α parameters (hypothesis *c*, assuming no displacements) are shown in Fig. 5. The maxima of intensity occur at the 100 and 110 positions as in an $L1_2$ structure for the Ni–Cr, and at $1\frac{1}{2}0$ positions for the Fe–Cr pair. For the Fe–Ni pair the maxima of diffuse scattering are located around Bragg peaks.

VII. Accuracy of short-range-order pair parameters

We now discuss the errors made on the α correlation parameters. They have three main origins: (*A*) the errors due to the reduction of experimental data to scattering cross section units; (*B*) the errors due to the statistical errors on measurements, and their influence on Fourier coefficients a_{lmn}; (*C*) the errors related to the resolution of linear equations $\mathbf{a}_{lmn} = A\boldsymbol{\alpha}_{lmn}$.

(*A*) According to formula (11), the differential coherent scattering cross section depends on: (1) the Debye–Waller factor; (2) the incoherent differential cross section of samples; (3) the normalization factor EUFAC.

(1) The three components of the alloy being close together in the periodic table, an average common value of the Debye–Waller factor is chosen. The complete analyses have been done with two extreme values of the Debye–Waller factor, 0·35 and 0·50, chosen to bound the experimental value of the disordered-Ni_3Fe Debye–Waller factor (0·40 Å^2). The results are unaffected by using either 0·35 or 0·50.

(2) The incoherent diffuse scattering cross section σ_{inc}, calculated from the isotopic and impurity composition of each sample, is particularly large for the third alloy. It is similar to a background noise, and an error on σ_{inc} affects only the first term of the Fourier transform (a_{000}, or α_{000}).

(3) The errors on the normalization factor EUFAC may be significant, since this factor is proportional to the difference between the vanadium and background intensities. The vanadium diffuse intensity is weak because a hollow cylinder is used to avoid multiple scattering.

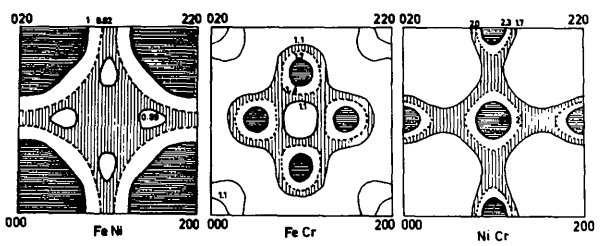

Fig. 5. Pair short-range-order diffuse intensity maps, synthesized with the first eight α^{AB}_{lmn}. Modified Sparks & Borie method and hypothesis *c* have been used.

Assuming the same relative error on the normalization factor $\pm\delta(EU/EU$ for any sample, the resulting relative error on the pair short-range-order parameter set is

$$\Delta(\alpha^{ab}_{lmn}) = \mp[\delta(\mathrm{EU})/\mathrm{EU}]\alpha^{ab}_{lmn} \qquad (17)$$

for any pair *ab*, and $lmn \neq 000$.

For $lmn = 000$, the error is increased by the term

$$\Delta\boldsymbol{\alpha}^{\mathrm{pair}}_{000} = [\delta(\mathrm{EU})/\mathrm{EU}]A^{-1}\boldsymbol{\sigma}^{\mathrm{inc}}_{\mathrm{Inox}}/4\pi, \qquad (18)$$

A being the contrast matrix. A qualitative idea of the errors on EUFAC may be obtained by comparison between the values of a_{000} and the total Laue value of each sample.

(*B*) The errors induced by the BS procedure of separation of short-range order and displacement intensities has been discussed in § V, leading to the conclusion that the size effects are small enough to introduce diffuse scattered intensity less that the statistical errors in the total diffuse scattering.

The evaluation of these statistical errors on direct intensity measurements has been given before (§ IV*B*). They introduce errors on the a_{lmn} coefficients, which have been computed with an expression similar to that given by Auvray, Georgopoulos & Cohen (1981). The standard deviation, due to counting statistics, of the a_{lmn} parameters are given in Table 4, in units of the last digit, for case *c* (displacement terms neglected).

The coefficients a_{000} should equal the total Laue monotonic values. Discrepancies from these expected values are very weak (compare Tables 2 and 4). The largest relative error reaches only 4% in case *c*. The results seem fairly accurate in spite of the weakness of scattered intensities.

To test the physical meaning of the values of the coefficients a_{lmn}, the short-range-order intensity has been synthesized using an increasing number of parameters and compared to the experimental averaged diffuse intensity. The resulting agreement ratios are shown in Fig. 6. It is clear that, for the three samples, the first two a_{lmn} have a physical meaning, but not the other ones.

(*C*) The resolution of the linear equations $a_{lmn} = A\alpha_{lmn}$ gives an amplification of the errors on the coefficients α_{lmn} which depends on the conditioning of the contrast matrix *A*. In this experiment, an error of 4% on a_{000} (case *c*) introduces an error of 5% on α_{000} (Tables 4 and 5).

Knowledge of the standard deviations due to counting statistics $\sigma(a^i_{lmn})$ allows us to compute the corresponding standard deviation of the α^{AB}_{lmn}, using $\mathbf{T} = \mathbf{A}^{-1}$, the inverse matrix of the contrast matrix. Then,

$$\sigma(\alpha^i_{lmn}) = \left[\sum_j t^2_{ij}\sigma^2(a^j_{lmn})\right]^{1/2}. \qquad (19)$$

These standard deviations are given in Table 5, for

case c; they are much smaller than those evaluated by the Turing relation. As should be expected from pair Laue values, the accuracy is largest for the Fe–Ni pair and smallest for the Fe–Cr pair.

A slight modification of scattering lengths b, which are known with an accuracy which varies from one isotope to another, induces a variation of the matrix A, and thus of the α parameters. As we have chosen the b scattering lengths so as to have the best values of α_{000}, we have to test the effect of b variation on the coefficients α_{lmn}. By changing the scattering lengths of the isotopes ^{52}Cr, ^{62}Ni, ^{58}Ni and ^{54}Fe by 0·12, 1·7, 0·17 and 0·45%, respectively, the Laue intensities change by less than 2·7%. The resulting errors on the significant α_{lmn} are smaller than the statistical ones by an order of magnitude except for α_{000}. These errors on α_{000} are 2, 11 and 4%, respectively, for the pairs Fe–Ni, Fe–Cr and Ni–Cr.

VIII. Conclusion

In this ternary alloy, there is short-range order between nickel and chromium. Despite the relatively large values of the Cowley parameters α_{110}^{NiCr} and α_{200}^{NiCr}, the correlation range is short and one can consider that the other Ni–Cr short-range-order pair parameters are zero. There is a small correlation of iron and chromium, and it is possible that iron-rich clusters exist in the alloy, as suggested by α_{110}^{FeNi}, which is known much more precisely than α_{110}^{FeCr}, and also by a preliminary experiment of small-angle neutron scattering we have made with these alloys. There is no tendency of short-range order between iron and nickel, in contrast with the well known tendency of iron and nickel to order in the f.c.c. solid solution (Wakelin & Yates, 1953; Lefebvre, Bley, Fayard & Roth, 1981; Paulevé, Dautreppe, Laugier & Néel, 1962; Roth, Chamberod & Billard, 1978). This may be compared with the strong decrease in critical ordering temperature of Ni_3Fe for chromium additions (13 K per 1% Cr) (Ferjani, 1978). The tendency of Cr to order with Ni leads to a strong decrease of the Fe–Ni interaction.

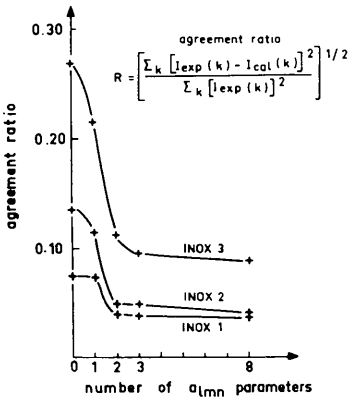

Fig. 6. Agreement ratio R for short-range-order intensity synthesized using $a_0 \rightarrow a_n$, compared to experimental I_{SRO} obtained in case c, with the modified method of separation.

The range of short-range ordering is confirmed by the observation of isolated pairs of dislocations is stainless-steel-type alloys.

A second consequence of the value of the correlation length is that the kinetic considerations used by Bendick & Pepperhoff (1981) to exclude local atomic arrangement as an explanation of the 873 K specific-heat anomaly must be reinvestigated.

A third consequence is that resistivity measurements are suitable to detect, in this case, the state of short-range order: in fact, resistivity changes are mainly due to the modification of the first and second shells, in contrast to the diffuse intensity which integrates all the Fourier contributions α_{lmn} of short-range order.

The authors are pleased to thank Professor M. Fayard for helpful suggestions and comments.

We are also grateful to C. Prevost for his help in preparing the single crystals and also to Dr N. Lehner for his assistance during the diffraction experiment.

APPENDIX

X-ray diffuse scattering

The development of high-energy storage rings gives the possibility of analysing local order in multicomponent alloys. The possibility of obtaining any chosen wavelength allows one to take advantage of the high variation of structure factor near absorption discontinuities. The aim of this Appendix is to develop some points which are specific to the analysis of ternary alloys, and to provide some implements for deciding whether X-ray measurements are possible with a given alloy.

As a consequence of the angular variation of the scattering factors, 54 of the 57 periodic functions $\tilde{\alpha}$, Q, R, S have to be separated and independently known. The contrast variation necessary for this separation may be obtained in two ways: the variation of the scattering factors with the radiation wavelength and the angular variation of the scattering factors. The first method is used in the Borie–Sparks-like method and the second in the Tibballs-like method.

(*A*) *The six-wavelength method*

This method is directly derived from the BS treatment (Borie & Sparks, 1971; Gragg & Cohen, 1971) but avoids some of its drawbacks.

In order to allow a quantitative comparison between the conceptual method developed here and its experimental efficiency, we have calculated the values of anomalous dispersion correction for some

elements. They have been computed from the Parratt & Hempstead (1954) theory, using the oscillator strength data given by Cromer (1965). The computed values show good agreement with those computed by Cromer (1965) at particular wavelengths, as well as with those measured by Bonse & Materlik (1976), for example on Ni at $\Delta\lambda/\lambda_K \simeq 10^{-2}$.

If we require all the displacement terms and all the SRO terms, without using the angular variation of the scattering-factor method, then we have to undertake six experiments with six different wavelengths. This number of wavelengths is equal to the number of wavelength-independent scattering-factor 'groups' appearing in (1) after transformations such as

$$[f_A(\mathbf{h})f_B^*(\mathbf{h}) + f_A^*(\mathbf{h})f_B(\mathbf{h})] = -|f_A(\mathbf{h}) - f_B(\mathbf{h})|^2 + |f_A(\mathbf{h})|^2 + |f_B(\mathbf{h})|^2,$$

for example, which lead to the following expression for intensity:

$$\begin{aligned} I_\lambda(\mathbf{h}) = {} & |f_A(\mathbf{h}) - f_B(\mathbf{h})|_\lambda^2 T_1(\mathbf{h}) + |f_A(\mathbf{h}) - f_C(\mathbf{h})|^2 T_2(\mathbf{h}) \\ & + |f_B(\mathbf{h}) - f_C(\mathbf{h})|^2 T_3(\mathbf{h}) + |f_A(\mathbf{h})|^2 T_4(\mathbf{h}) \\ & + |f_B(\mathbf{h})|^2 T_5(\mathbf{h}) + |f_C(\mathbf{h})|^2 T_6(\mathbf{h}), \end{aligned} \tag{A1}$$

where

$$\begin{aligned} T_1(\mathbf{h}) = {} & x_A x_B [\tilde{\alpha}^{AB}(\mathbf{h}) - h_I Q_I^{AB}(\mathbf{h}) - (h_I)^2 R_I^{AB}(\mathbf{h}) \\ & - h_I h_J S_{I,J}^{AB}(\mathbf{h})] \end{aligned} \tag{A2}$$

$$\begin{aligned} T_4(\mathbf{h}) = {} & (x_A)^2 [h_I Q_I^{AA}(\mathbf{h}) + (h_I)^2 R_I^{AA}(\mathbf{h}) \\ & + h_I h_J S_{I,J}^{AA}(\mathbf{h})] + x_A x_B [h_I Q_I^{AB}(\mathbf{h}) \\ & + (h_I)^2 R_I^{AB}(\mathbf{h}) + h_I h_J S_{I,J}^{AB}(\mathbf{h})] \\ & + x_A x_C [h_I Q_I^{AC}(\mathbf{h}) + (h_I)^2 R_I^{AC}(\mathbf{h}) \\ & + h_I h_J S_{I,J}^{AC}(\mathbf{h})] \end{aligned} \tag{A3}$$

and similar expressions for the others.

The main advantage of this decomposition of intensity is that it differentiates the six T_i functions which characterize order and depend on the scattering vector $\mathbf{h}$ from the six scattering-factor 'groups' which contain all the wavelength dependence of the intensity. Let us define, for a given set (h_1, h_2, h_3) an intensity column vector $\mathbf{I}$ whose components I_j account for a measurement at a particular wavelength λ_j and let $\mathbf{T}$ be the column vector of component T_i previously defined, each component being the equivalent of the binary BS expression.

Equation (A1) will now be written in matrix form:

$$\mathbf{I} = C_M \mathbf{T} \quad \text{or} \quad \mathbf{T} = C_M^{-1} \mathbf{I}, \tag{A4}$$

where C_M is the contrast matrix.

To construct the intensity vector in the BS measurement volume, each component T_i of the $\mathbf{T}$ vector is separated by inverting the contrast matrix for each point $(h_1 h_2 h_3)$. Then the T_i components are analysed following the binary procedure yielding a value for each individual parameter. The six wavelengths have to be chosen so that they produce a well-conditioned linear system for all reciprocal space. This method is applicable to alloys such that each element has an absorption edge in the wavelength range from about 0·5 to 2 Å. The wavelengths are then chosen on both sides of these absorption edges.

Table 6. *Associated Turing number $N(C_M)$ and determinant of normalized matrix for the contrast matrix* (Fe–Cr–Ni *alloy*)

	Set 1		Set 2	
$\sin\theta/\lambda$	$N(C_M)$	Determinant	$N(C_M)$	Determinant
0·1	105	5×10^{-7}	64	2×10^{-6}
0·3	47	9×10^{-6}	28	4×10^{-5}
0·5	19	2×10^{-4}	12	9×10^{-4}

Here, we consider the case of the Ni–Fe–Cr alloy. This method would be clearly applicable since there are pronounced varations in the dispersion corrections close to the K edges (Fig. 7). The wavelengths of the K absorption edges of pure Ni, Fe and Cr are respectively 1·488, 1·743 and 2·070 Å. We have used two sets of wavelengths to test the method:

first set: $\lambda_1 = 1{\cdot}470$, $\lambda_2 = 1{\cdot}493$, $\lambda_3 = 1{\cdot}739$, $\lambda_4 = 1{\cdot}900$, $\lambda_5 = 2{\cdot}065$, $\lambda_6 = 2{\cdot}200$ Å;

second set: λ_1, $\lambda_2' = 1{\cdot}489$, $\lambda_3' = 1{\cdot}741$, λ_4, $\lambda_5' = 2{\cdot}068$ Å, λ_6.

They are on both sides of the K edges and, for each element, one of the wavelengths is very close to the K edge ($\Delta\lambda \sim 5\times10^{-3}$ Å in the first set, $\Delta\lambda \sim 2\times10^{-3}$ Å in the second set). The Turing number of the contrast matrix and the determinant of the normalized matrix have been calculated for the two sets and for some values of $s = \sin\theta/\lambda$ (Table 6).

The accuracy of the method is improved when, for each element, one of the wavelengths is as close as possible to the K absorption edge; it is also improved when the volume of measurement is shifted towards greater values of s, but this is a limited possibility. These matrices are not very well conditioned, but it

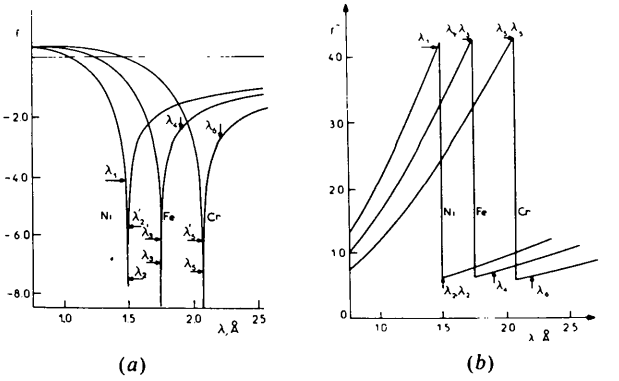

(*a*) (*b*)

Fig. 7. Real and imaginary part of the anomalous dispersion corrections for the elements Ni–Fe–Cr. The arrows indicate the precise wavelengths used in the calculation of the Turing number of Table 1.

is probably possible, with accurate measurements, to obtain good results.

The conditioning of the system Ni–Fe–Cr may be compared to that of the system Au–Ag–Cu. The wavelengths have been chosen on both sides of K absorption edges of Cu and Ag and of L absorption edges of Au; for $s = 0{\cdot}1$, the Turing number is $1{\cdot}4 \times 10^4$ and the determinant of the normalized matrix is 5×10^{-12}. In this system, it is clearly impossible to use this method of separation.

In some cases, if all displacement terms T_4, T_5, T_6 are not required, it may be expected that the number of experiments is reduced to three. The expression of the intensity has to be written, for example, as

$$\begin{aligned} I_{\lambda_i} = &|f_A(\mathbf{h}) - f_B(\mathbf{h})|^2_{\lambda_i} T_1(\mathbf{h}) + |f_A(\mathbf{h}) - f_C(\mathbf{h})|^2_{\lambda_i} T_2(\mathbf{h}) \\ &+ |f_B(\mathbf{h}) - f_C(\mathbf{h})|^2_{\lambda_i} T_3(\mathbf{h}) \\ &+ |f_A(\mathbf{h})|^2_{\lambda_i} [T_4(\mathbf{h}) + |f_B(\mathbf{h})/f_A(\mathbf{h})|^2_{\lambda_i} T_5(\mathbf{h}) \\ &+ |f_C(\mathbf{h})/f_A(\mathbf{h})|^2 T_6(\mathbf{h})]. \end{aligned} \quad (A5)$$

But for each experiment the wavelength is chosen to give an appreciable dispersion correction f' and f'' so that the ratios $|f_B/f_A|$ and $|f_C/f_A|$ are far from constant for the set of three experiments. As the $|f_A - f_B|^2_{\lambda_i}$ factors also have very different variations in reciprocal space, a correct separation of the pair short-range-order modulations is clearly impossible without assuming that displacement terms are negligible.

(B) *Methods derived from that of Tibballs*

This method (Tibballs, 1975) developed by Georgopoulos & Cohen (1977, 1981), may be directly generalized by the use of 54 functions instead of 25 in binary alloys. If only one wavelength is used, difficulties will arise because of the large size of the reciprocal volume to explore: one needs to reach the 620 reciprocal points, in the case of a f.c.c. disordered lattice, and it is likely that the higher-order displacement terms may not be neglected since they are multiplied by h^3 or h^4.

If more wavelengths are used, the Tibballs method may be generalized with a total volume of at least 54 minimal volumes. Here, the matrices to invert are 54×54.

A particular method, with two wavelengths, allows the inversion of smaller matrices (29×29). Measurements are carried out with two wavelengths on each side of the absorption edge of one of the elements A, and the difference $I(\lambda_1, \mathbf{h}) - I(\lambda_2, \mathbf{h})$ is analysed (Ramesh & Ramaseshan, 1971). The following criteria must be fulfilled for this method to be meaningful.

(1) λ_1 and λ_2 are short enough to be associated with measurement volumes equal to 29 'minimal volumes to repeat SRO' (instead of 25 in a binary Tibballs scheme).

(2) For any point in the measurement volume, the difference $I_{\lambda_1} - I_{\lambda_2}$ is sufficiently large to avoid redundant information from λ_1 and λ_2.

(3) The difference $\Delta\lambda$ between the two wavelengths is small enough that the variation of f' and f'' for the two other species B and C can be neglected.

The intensity difference may then be written

$$\begin{aligned} &I(\lambda_1, \mathbf{h}) - I(\lambda_2, \mathbf{h}) \\ &= x_A x_B |f_A(\mathbf{h}) - \bar{f}_B(\mathbf{h})|^2_{\lambda_1\lambda_2} \tilde{\alpha}^{ab}(\mathbf{h}) \\ &\quad + x_A x_C |f_A(\mathbf{h}) - \bar{f}_C(\mathbf{h})|^2_{\lambda_1,\lambda_2} \tilde{\alpha}^{AC}(\mathbf{h}) \\ &\quad + (x_A)^2 |f_A(\mathbf{h})|^2_{\lambda_1,\lambda_2} [h_I Q_I^{AA}(\mathbf{h}) + (h_I)^2 R_I^{AA}(\mathbf{h}) \\ &\quad + h_I h_J S_{I,J}(\mathbf{h})] \\ &\quad + x_A x_B [\bar{f}_B^*(\mathbf{h}) f_A(\mathbf{h}) + f_A^*(\mathbf{h}) \bar{f}_B(\mathbf{h})]_{\lambda_1\lambda_2} \\ &\quad \times [h_I Q_I^{AB}(\mathbf{h}) + (h_I)^2 R_I^{AB}(\mathbf{h}) + h_I h_J S_{I,J}^{AB}(\mathbf{h})] \\ &\quad + x_A x_C (\bar{f}_C^*(\mathbf{h}) f_A(\mathbf{h}) + f_A^*(\mathbf{h}) \bar{f}_C(\mathbf{h}))_{\lambda_1,\lambda_2} \\ &\quad \times [h_I Q_I^{AC}(\mathbf{h}) + (h_I)^2 R_I^{AC}(\mathbf{h}) + h_I h_J S_{I,J}^{AC}(\mathbf{h})], \end{aligned} \quad (A6)$$

where $(f_A)\lambda_1\lambda_2$ accounts for the difference $(f_A)\lambda_1 - (f_A)\lambda_2$, for example, and

$$\bar{f}_B = [f_B(\lambda_1) + f_B(\lambda_2)]/2 \simeq f_B(\lambda_1) \simeq f_B(\lambda_2).$$

In this expression there remain only 29 periodic functions. These may be separated by a Tibballs-like treatment – provided that f_A, f_B, f_C have sufficiently different angular dependences. These modulations are then introduced as input in the expression of $I(\lambda_1, \mathbf{h}) + I(\lambda_2, \mathbf{h})$, the remaining unknown modulations are separated following the same Tibballs-like treatment.

This method is well suited to alloys where A, B, C are separated in the Periodic Table and where A is sufficiently heavy that it has an L absorption edge in the range 0·5 to 1·5 Å. A good example is the Cu–Ag–Au alloy. As can be seen from Fig. 2, f' and f'' of Ag and Cu atoms are nearly constant in the wavelength range associated with the broad L absorption edge of Au. The terms neglected in the intensity difference expression are only 0·2 or 0·3% for the wavelengths indicated by arrows on Fig. 8. The suitability of a

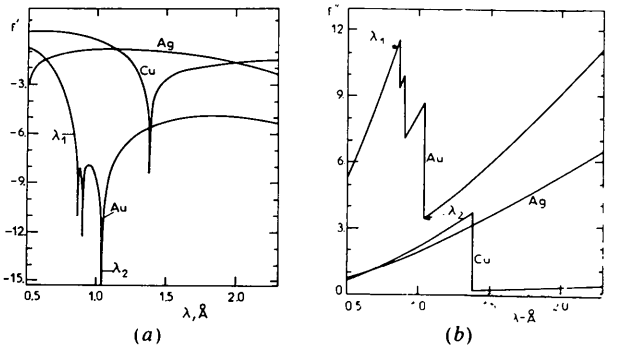

Fig. 8. Real and imaginary part of the anomalous dispersion correction for the elements Au–Ag–Cu.

Tibballs-like analysis depends on the variation of the ratios f_{Ag}/f_{Cu} with $\sin\theta/\lambda$. These values are similar to those in the CuAl binary case (Auvray *et al.*, 1981) and it seems possible to perform such an analysis.

(C) *Discussion*

It has been shown that there is no systematic method of analysis for X-ray scattering, each alloy having to be considered as a special case dictating the number of wavelengths to be used. However, two main kinds of analysis are pointed out; the six-wavelength method which correctly overcomes the difficulties arising from the atomic-scattering-factor variation with s and the mixed method which uses these variations to a large extent. Nevertheless, intrinsic difficulties must be overcome. Some of the wavelengths used must be as near as possible to the absorption edge, to enhance the contrast variation [for example $(\lambda-\lambda_K)/\lambda_K \sim 10^{-3}$) and, hence, a good wavelength reproducibility and a good discrimination ($\Delta\lambda/\lambda < 10^{-3}$) are needed. They also require precise knowledge of the absorption edges, the values of which are shifted, alloying producing a modification of the screening effect. So, in spite of the improvement in the theoretical computation of anomalous dispersion corrections (Cromer & Liberman, 1981), these latter must be experimentally determined.

References

AUVRAY, X., GEORGOPOULOS, P. & COHEN, J. B. (1981). *Acta Metall.* **29**, 1061–1075.

BELL, W., ROSER, W. R. & THOMAS, G. (1964). *Acta Metall.* **12**, 1247–1253.

BENDICK, W. & PEPPERHOFF, W. (1981). *J. Phys. F*, **11**, 57–63.

BONSE, U. & MATERLIK, G. (1976). *Z. Phys.* **B24**, 189–191.

BORIE, B. & SPARKS, C. J. JR (1971). *Acta Cryst.* **A27**, 198–201.

CROMER, D. T. (1965). *Acta Cryst.* **18**, 17–23.

CROMER, D. T. & LIBERMAN, A. (1981). *Acta Cryst.* **A37**, 267–268.

DIMITROV, C., TENTI, M. & DIMITROV, O. (1981). *J. Phys. F*, **11**, 753–765.

DOUGLASS, D. L., THOMAS, G. & ROSER, W. R. (1964). *Corros. Sci.* **20**, 15t–28t.

FERJANI, H. (1978). Thèse de 3ème cycle. Univ. P. et M. Curie, Paris.

FONTAINE, DE D. (1971). *J. Appl. Cryst.* **4**, 15–19.

GEORGOPOULOS, P. & COHEN, J. B. (1977). *J. Phys.* **38**, C7, 191–196.

GEORGOPOULOS, P. & COHEN, J. B. (1981). *Acta Metall.* **29**, 1535–1551.

GRAGG, J. E. JR (1970). Doctoral Dissertation, Northwestern Univ., Evanston, IL, USA.

GRAGG, J. E. JR & COHEN, J. B. (1971). *Acta Metall.* **19**, 507–519.

HAYAKAWA, M. & COHEN, J. B. (1975). *Acta Cryst.* **A31**, 635–645.

HIRABAYASHI, M., KOIWA, M., YAMAGUCHI, S. & KAMATA, K. (1978). *J. Phys. Soc. Jpn*, **45**, 1591–1598.

KOESTER, L. & RAUCH, H. (1981). *Summary of Neutron Scattering Lengths.* IAEA Contract Report 2517/RD. Vienna: IAEA.

LEFEBVRE, S., BLEY, F., FAYARD, M. & ROTH, M. (1981). *Acta Metall.* **29**, 749–761.

LEFÈVRE, A. (1980). Rapport de Microthèse, ENSCP, Paris.

METCALFE, E. & LEAKE, J. A. (1975). *Acta Metall.* **23**, 1135–1143.

NAKASHIMA, T., MIZUNO, S., IDO, T., SATO, K., MITANI, S. & ADACHI, K. (1977). *J. Phys. Soc. Jpn*, **43**, 1870–1878.

PARRATT, L. G. & HEMPSTEAD, C. F. (1954). *Phys. Rev.* **94**, 1593–1600.

PAULEVÉ, J., DAUTREPPE, D., LAUGIER, J. & NÉEL, (1962). *J. Phys. Radium*, **23**, 841–843.

PEARSON, W. B. (1958). *Handbook of Lattice Spacing and Structures of Metals.* London: Pergamon.

PELLETIER, J. M. (1981). Private communication.

PROTOPOPOFF, E. (1981). Rapport de DEA. Univ. P. et M. Curie, Paris.

RAMESH, T. G. & RAMASESHAN, S. (1971). *Acta. Cryst.* **A27**, 569–572.

ROTH, M., CHAMBEROD, A. & BILLARD, L. (1978). *J. Magn. Magn. Mater.* **7**, 104–106.

SCHURMANN, E. & BRAUCKMANN, J. (1977). *Arch. Eisenhuettenwes.* **48**, 3–7.

TIBBALLS, J. E. (1975). *J. Appl. Cryst.* **8**, 111–114.

WAKELIN, R. J. & YATES, E. L. (1953). *Proc. Phys. Soc. London Sect. B*, **66**, 221–240.

WARNES, L. A. A. & KING, H. W. (1976). *Cryogenics*, **16**, 479–481, 659–667.

WELLS, P. & SMITH, J. H. (1971). *J. Phys. F*, **1**, 763–770.

WESTLAKE, J. (1968). *A Handbook of Numerical Matrix Inversion and Solution of Linear Equations.* New York: Wiley.